X-ray photoelectron diffraction of NiO: Experiments and calculations in an extended single-scattering-cluster model

C. Scharfschwerdt, T. Liedtke, and M. Neumann
Fachbereich Physik, Universität Osnabrück, D-49069 Osnabrück, Germany

T. Straub and P. Steiner
Fachbereich Physik, Universität des Saarlandes, D-66123 Saarbrücken, Germany
(Received 12 March 1993; revised manuscript received 7 June 1993)

We present a set of polar-angle-dependent x-ray photoelectron spectroscopy (XPS) measurements obtained from single-crystalline NiO, *in situ* cleaved and ion bombarded. The intensities of the O 1*s* and Ni 2*p* XPS peaks show characteristic x-ray photoelectron diffraction effects with intensity maxima in the low-index directions (e.g., [001], [101], [102], and [103]). The relative height of the maxima can partly be deduced from crystal geometry and scattering strength of O and Ni (derived from the atomic scattering factors), where O is a much weaker scatterer than Ni. Nevertheless it turns out that O plays an important role as a scatterer in these experiments, especially considering the O 1*s* emission along [101]. Experimental observations are compared to calculations for an improved single-scattering-cluster (SSC) model including a simulation of multiple scattering. This addition turned out to be necessary in order to get reasonable agreement of experiment and calculation while still retaining most of the ease and clarity of the original SSC model.

I. INTRODUCTION

The intensity of x-ray photoelectron spectroscopy (XPS) signals from ordered structures depends systematically on the direction into which the electrons are emitted. This effect is known for about 20 years since the pioneering work of Siegbahn and co-workers[1,2] on NaCl and is commonly described as x-ray photoelectron diffraction (XPD). During the last years a number of attempts to understand and to quantify the observations have been carried out (see reviews in Refs. 3–8). The basic phenomenon is elastic scattering of the outgoing photoelectron on the surrounding (effective) atomic potentials.[9] The typical energy for this kind of experiments is well above a few hundred eV. In this energy regime scattering on an atom leads to an enhancement of the intensity for small scattering angles.[10,11] This forward scattering can also be described as "forward focusing" because the scattering atom acts like a focusing lens for the electron passing by.[12] Maxima in the intensity variation can in principle be attributed to directions of neighboring atoms and thus give information on the structure of the surface region. Besides this, forward focusing can have a significant influence on the quantification of XPS data as shown in Ref. 13.

In this work we will present XPD spectra of cleaved NiO surfaces obtained under various polar and azimuthal angles. We will try to give an explanation for the observations and compare the spectra to calculations within the single-scattering-cluster (SSC) model. We will present an approach taking into account effects of multiple scattering which gives a much better agreement with the experiment.

II. EXPERIMENT

The measurements presented here were carried out in a VG ADES-400 angle resolving spectrometer equipped with a dual x-ray anode at a base pressure of about 10^{-10} mbar. This machine is equipped with a movable analyzer that can be rotated within two perpendicular planes. In all the experiments the direction of the incident light was kept fixed with respect to the sample at an angle of 72° to the surface normal. The detector direction (and thus the exit direction of the electrons) was varied by moving the analyzer. A sketch of the geometry is shown in Fig. 1. Except for two spectra, all measurements were carried out in the plane defined by the direction of the incoming light and the surface normal. The angular resolution for our system is about 2.5°. The energy resolution is about

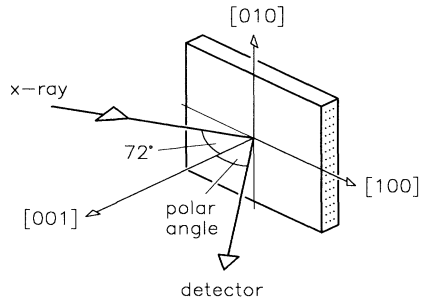

FIG. 1. Experimental geometry for the measurements in the (010) plane. Additionally the analyzer can be tilted perpendicular to the indicated plane.

0.7 eV at a pass energy of 50 eV. Al Kα ($\hbar\omega$ = 1486.7 eV) was used for excitation.

Single-crystalline surfaces of NiO were prepared by cleaving *in situ* (UHV conditions) with a specially designed tool. By this procedure we obtain nearly perfect and absolutely clean (001) surfaces (cf. Refs. 14 and 15).

III. EXPERIMENTAL RESULTS

All measurements were carried out on cleaved (001) surfaces of NiO single crystals. The data presented here were obtained by measuring O 1*s* and Ni 2*p* XPS spectra as a function of the polar angle of the emitted electrons. The kinetic energies of the main peaks are 632 eV for Ni 2*p* and 955 eV for O 1*s* (see Fig. 2). The presented XP spectra are shifted to lower kinetic energies due to static sample charging as NiO is an insulator.

In the following we will use the term "XPD spectrum" for the intensity of the corresponding XP spectrum as a function of the polar angle (with respect to the surface normal). Each point in the XPD spectrum was obtained from a complete XPS spectrum. The intensity was determined from the peak area after subtracting the inelastic background with an algorithm developed by Tougaard (see, e.g., Ref. 16). For the measurements obtained from the sputtered sample we took the maximum intensities (after background subtraction). The resulting spectra were smoothed using cubic splines. Both data and splines are presented in the figures. Except for two data sets all XPD spectra presented here were measured within the (010) plane (perpendicular to the sample surface).

A. Cleaved NiO surface

In Fig. 3 XPD spectra for O 1*s* and Ni 2*p* in two different azimuths are shown. The step width for these spectra is 1°. As it turned out that the intensity variations are more pronounced when the sample is cooled down, the following measurements were carried out at T = 90 K (liquid nitrogen temperature). Within our energy resolution, which is mainly determined by the linewidth of the nonmonochromatic x-ray light, we found no evidence for adsorption of OH on the clean surfaces. (Adsorbed OH groups lead to a satellite feature 1.8 eV apart from the main line.[15]) (010) in Fig. 3 indicates the (010) azimuth. The two measurements labeled $1\bar{1}0$ were obtained by simultaneously varying both analyzer angles. This movement is along $1\bar{1}0$ for small angles and deviates a bit for larger angles. This deviation was taken into account in the calculations shown later and, for a qualitative discussion, this is close enough to $1\bar{1}0$.

All four XPD spectra exhibit a clear variation as a function of the polar angle. They all show a pronounced maximum in normal emission. Besides this the (010) spectra show maxima between 20° and 30° and around 45°, whereas the $1\bar{1}0$ spectra show a broad structured maximum at around 35° and a weaker one between 50° and 60°. Another point worth mentioning is that the spectra are not symmetric with respect to the surface normal (as far as can be seen from the angular range shown here). For higher angles the intensity drops.

To show the connection between these measurements and the crystal geometry, we plotted the spectra as polar plots in Figs. 4 and 5, together with a cut through the crystal in the plane of the measurements. The emitting atom is situated in the lower left of each figure, lines indicate directions to the nearest neighbors.

B. Ion-bombarded NiO

Figure 6 shows the influence of argon ion bombardment on the XPD spectra. Sputtering destroys (or at least disturbs) the surface ordering. On the other hand it is known that lighter O atoms are expelled more easily than heavier Ni atoms (preferential sputtering was reported in Refs. 17 and 18). So it is interesting to look at the changes in the XPD spectra.

The sample was sputtered at room temperature by 3 keV Ar ions (incident perpendicular to the surface) for several minutes in the first case and for another few minutes in the second case. This led to changes in the O 1*s* XPS spectrum [shown in Fig. 7(a)]. At lower kinetic energy an additional structure appears. The intensity of this satellite varies smoothly and does not exhibit any pronounced features. The intensity of the satellite was calculated from curve fits as indicated in Fig. 7(a).

Along with this the Ni 2*p* XPD spectrum gets washed out. After the second sputtering the only prominent fea-

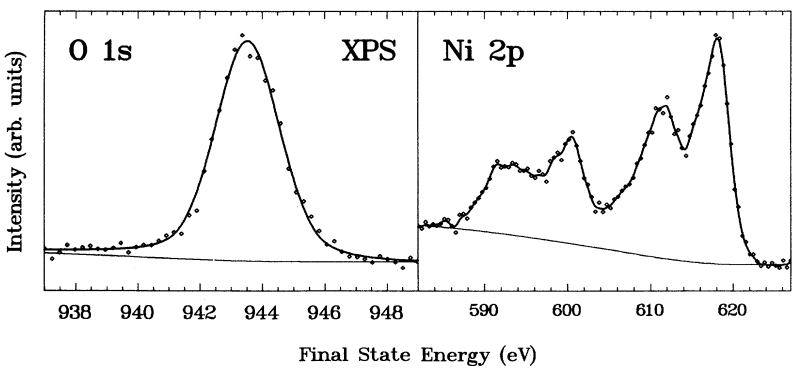

FIG. 2. XP spectra of Ni 2*p* and O 1*s* in normal emission. These data are not corrected for sample charging. The background that was subtracted to determine the intensity is indicated.

ture remaining is the maximum at 0°. The changes in the O 1s XPD spectrum are a bit less pronounced but a weakening of the structure is also clearly observable.

IV. DESCRIPTION OF THE THEORETICAL MODEL

The model we used to describe our observations is based on the well-known single-scattering-cluster model (SSC) introduced, for example, in Refs. 19 and 20. This model has been shown to be in very good agreement with a wide range of XPD experiments (see, e.g., Ref. 21). However, it has mainly been applied to metals and metal-adsorbate systems so far.

Within this model the intensity emitted from an atom i and scattered by the atoms j (see Fig. 8) into the direction $\mathbf{r}_{\mathrm{det}}$ of the detector is given by

$$\left| \sqrt{\frac{d\sigma}{d\Omega}(\Theta(\mathbf{r}_{\hbar\omega},\mathbf{r}_{\mathrm{det}}))}\, e^{\frac{-l_i}{2\lambda}} + \sum_j \sqrt{\frac{d\sigma}{d\Omega}(\Theta(\mathbf{r}_{\hbar\omega},\mathbf{r}_{ij}))}\, f_{ij}^{\mathrm{eff}} e^{-\frac{l_j}{2\lambda}} e^{-ik\Delta_{ij}} \right|^2 \tag{1}$$

where $\Theta(\mathbf{r}_i,\mathbf{r}_j)$ denotes the angle between two vectors $\mathbf{r}_i$ and $\mathbf{r}_j$, $\mathbf{r}_{ij}$ is the vector $\mathbf{r}_j - \mathbf{r}_i$ pointing from atom i to j, Δ_{ij} is the projected path length difference in detector direction between positions i and j. $\frac{d\sigma}{d\Omega}(\Theta)$ is the photoionization cross section as given in[22,23]

$$\frac{d\sigma}{d\Omega}(E,\Theta) = \frac{\sigma_{nl}(E)}{4\pi}\left(1 - \frac{\beta}{4}(3\cos^2\Theta - 1)\right). \tag{2}$$

The values for β were taken from Ref. 24, $\sigma_{nl}(E)/4\pi$ was neglected because it can be factored out of Eq. (1) and it is not angle-dependent. Equation (2) describes the dependence of the intensity, so we put the square root of $d\sigma/d\Omega$ into Eq. (1) because the sum is carried out for the amplitude. The term $e^{-l/2\lambda}$ describes the attenuation of the amplitude (intensity $\propto e^{-l/\lambda}$) connected to inelastic losses (l_i is the distance from the atom i to the surface along $\mathbf{r}_{\mathrm{det}}$).

The effective scattering factor f_{ij}^{eff} (not to be intermixed with the f_{eff} defined by Rehr *et al.*[25,26] that is mentioned below) describes the scattering of an electron moving from atom i to atom j and scattered into the direction $\mathbf{r}_{\mathrm{det}}$. It is given by

$$f_{ij}^{\mathrm{eff}} = e^{-\frac{|\mathbf{r}_{ij}|}{2\lambda}} e^{ik|\mathbf{r}_{ij}|} \frac{f_j(\Theta(\mathbf{r}_{ij},\mathbf{r}_{\mathrm{det}}))}{|\,\mathbf{r}_{ij}\,|} \mathrm{DW}(\Theta(\mathbf{r}_{ij},\mathbf{r}_{\mathrm{det}})). \tag{3}$$

$f_j(\Theta)$ is the complex scattering factor for the scattering of the electron by atom j. It was taken from the tables in Refs. 10 and 11 which contain calculations (numerical solutions of the Dirac equation) for plane wave scattering (partial wave expansion) on atomic potentials. DW(Θ) is the Debye-Waller factor. The Debye temperature of 577 K was taken from Ref. 27 (for the topmost surface layer we used half of this value in the calculations). Up to this point our description follows the standard SSC model with just some terms in Eq. (1) grouped differently. Because we will use f_{ij}^{eff} in the extension described below it was necessary to introduce the whole formalism.

Additionally refraction of the outgoing electrons on the surface was included by assuming an inner potential of 6.7 eV as derived from angle-resolved ultraviolet photoelectron spectroscopy measurements.[28]

The above summation over j is carried out for all atoms in the cluster which in our case was a cuboid of 7 by 7 by 4 unit cells, each containing 4 Ni and 4 O atoms. This sum is the total intensity from one emitter. The summation over the emitters only has to be carried out for all inequivalent atoms in the cluster.

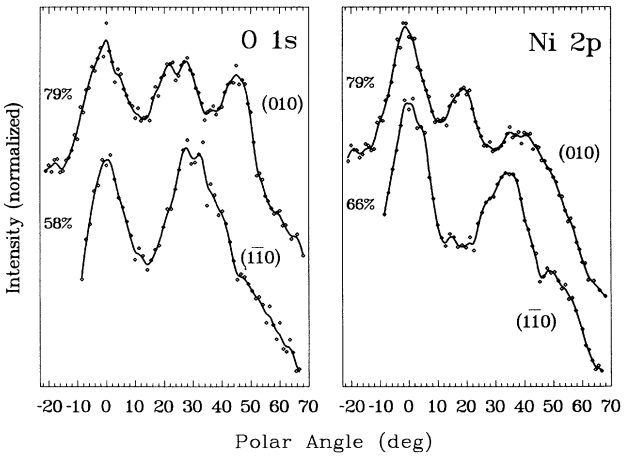

FIG. 3. XPS intensities for O 1s and Ni 2p as a function of the polar angle (= XPD). The amount of modulation is indicated as a percentage $[(Y_{\mathrm{max}} - Y_{\mathrm{min}})/Y_{\mathrm{max}}]$. Thick lines are smoothing splines, step size is 1°.

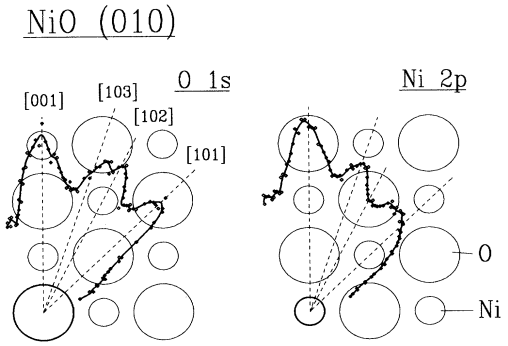

FIG. 4. Polar plots of the XPD spectra from Fig. 3 in the (010) azimuth. The straight lines point to the nearest neighbors.

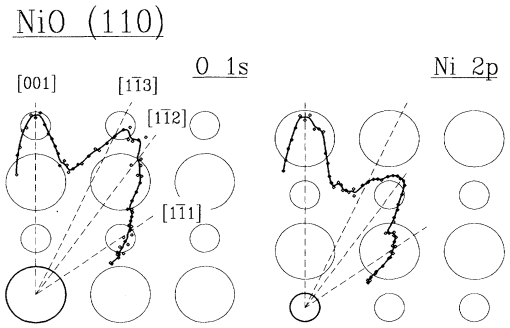

FIG. 5. Polar plots of the XPD spectra from Fig. 3 in the $1\bar{1}0$ azimuth.

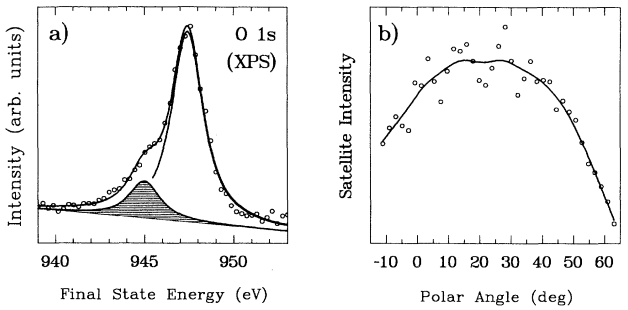

FIG. 7. (a) O 1*s* spectrum (XPS) after the first ion bombardment. (b) Intensity of the "satellite" as a function of angle.

A. Extensions to the SSC model

There are two main shortcomings of this model. One is that electrons are treated as plane waves instead of spherical waves and the other is the neglection of multiple scattering. A correct treatment of spherical waves tends to decrease forward-scattering amplitudes.[25,26] A usual approach to approximate this influence is to decrease the above-mentioned scattering factors $f_j(\Theta)$. This was also done in our calculations.

The most important and visible influence of multiple scattering is that it reduces forward focusing along chains of atoms. This has been shown in calculations by Tong, Poon, and Snider[29] and Xu, Barton, and van Hove[30] as well as in experiments by Egelhoff.[31] The clearest explanation for this can be found in the "forward focusing" model introduced by Tong, Poon, and Snider. The atomic potential acts like a focusing lens for the scattered electron. Extending this analogy it can easily be seen that a number of lenses which are lined up will in most cases end up in a defocusing arrangement.

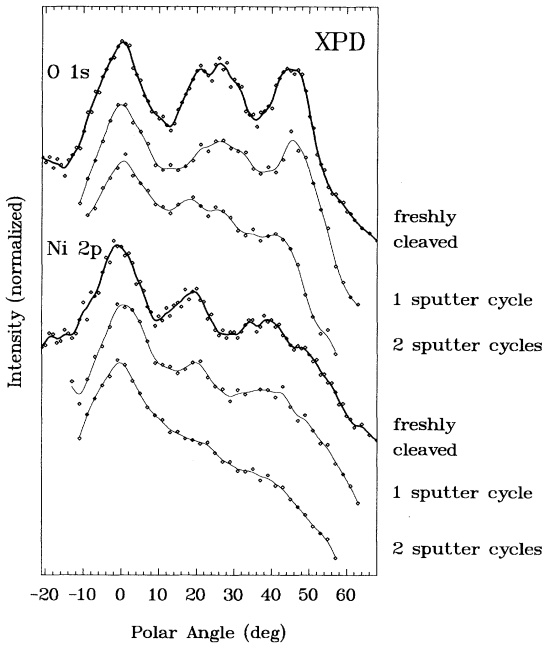

FIG. 6. XPD spectra of NiO after ion bombardment: the topmost curve shows the undisturbed curve. The measurement plane is (010). Step size is 2° for the data obtained from the sputtered sample.

However, multiple-scattering calculations are complicated and time consuming. So, in order to simulate these effects in our calculations we added a routine to the program that looks up whether atoms are lined up from the emitting atom in the direction of the detector (within an angle of $\pm\Delta\Theta$). If this is the case, only the scattering on the first atom in the chain is taken into account. The defocusing is introduced by scaling this scattering down by a factor of $(1 + c_{\text{mult}} \sum_j f_{ij}^{\text{eff}\,2})^{-1}$. The summation is carried out for the rest of the atoms in the line. By variation of c_{mult} the influence of this correction can be adjusted. The values used in our calculations are $c_{\text{mult}} = 1.0$ and $\Delta\Theta = 10°$. These were chosen so that the (calculated) emission from a chain of Ni atoms resembles that from the dynamical calculations of Xu, Barton, and von Hove.[30] With this method we can deduce the influence of multiple scattering from a rather simple calculation for a linear chain and transfer it to the more complicated cluster calculation.

The parameters used in the calculations are described in the following. We derived the inelastic mean free path λ from the equation given by Tanuma, Powell, and Penn.[32] For O 1*s* ($E_{\text{kin}} \approx 955$ eV) the value calculated in this way is 17.8 Å, for Ni 2*p* ($E_{\text{kin}} \approx 632$ eV) it is 13.1 Å. The asymmetry factor β in Eq. (2) is 2 for O 1*s* and 1.424

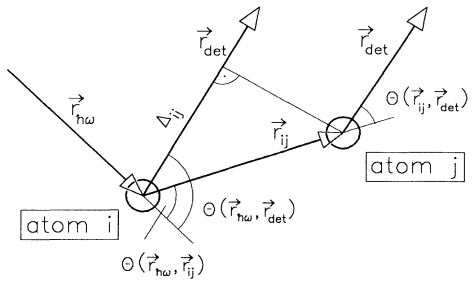

FIG. 8. The geometry of the basic scattering event in the SSC calculation: an electron is emitted from atom *i* and scattered on atom *j*.

for Ni $2p$.[24] The angle of incidence for the exciting x ray is 72°. In none of the shown calculations did we account for an angular broadening due to finite angle resolution in the measurement.

V. DISCUSSION

A. Influence of the photoionization cross section

A bit surprising at first glance might be that the observed XPD spectra do not show the complete symmetry of the crystal structure (which is a rock salt structure). From this we would expect symmetry around normal emission. This is true as long as only the crystal in itself is considered. In the experiment the incident light breaks the symmetry. The angle of incidence is −72° with respect to the surface normal. According to Eq. (2) the photoionization cross section has a maximum at 90° (to the incidence), that is 18° on our scale. So to the left of the normal emission the intensity is stronger reduced than on the right-hand side. This effect can be studied by varying the angle of incidence. Indeed the relative intensities shift while the peak positions stay at the same place (not shown here).

As can be seen in Eq. (1) the influence of $\frac{d\sigma}{d\Omega}(\Theta)$ cannot simply be factored out because the arguments $\Theta(\mathbf{r}_{\hbar\omega}, \mathbf{r}_{\rm det})$ and $\Theta(\mathbf{r}_{\hbar\omega}, \mathbf{r}_{ij})$ are different. However, only those directions close to the direct emission contribute significantly to the amplitude. So, to obtain an estimation of the influence of the photoionization cross section we divided the XPD spectra from Fig. 3 by $\frac{d\sigma}{d\Omega}(\Theta)$. The result is shown in Fig. 9. The O $1s$ spectrum looks more or less symmetric now, but the Ni $2p$ seems to be skewed just the other way around as before. This indicates that the β value used in Eq. (2) might be too large. When it is reduced to about 0.9 the spectrum looks much more symmetric. The lowering of β is reasonable because the value presented in Ref. 23 were calculated for free atoms in opposition to atoms in a solid examined here. Ebel and Jablonski showed that β values for emission from solids get significantly reduced compared to atomic values due to elastic scattering.[33,34] They derived a formula to calculate a corrected β, which would result in $\beta \approx 0.8$ for Ni $2p$. Their proposed correction depends on the atomic number and is close to the original $\beta = 2$ for O. So this is in good agreement with our observations.

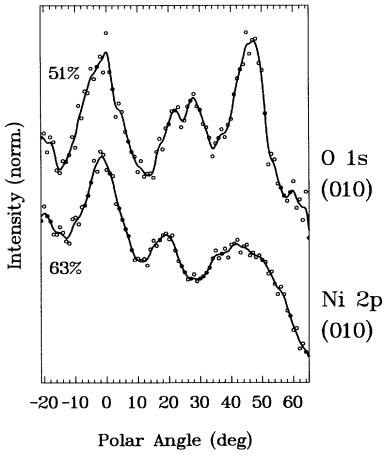

FIG. 9. XPD spectra from Figure 3 [(010) plane] corrected by $d\sigma(\Theta)/d\Omega$ [Eq. (2)].

B. Cleaved NiO surface

Many of the diffraction effects modulating the XPD spectra shown above can be modeled from the very basic scattering events where only the scattering of the outgoing electron on the two or three nearest-neighboring atoms is taken into account. This has been shown for example by Poon and Tong[12] (theoretically) and Armstrong and Egelhoff[35,31] (experimentally).

The most important feature of the scattering of electrons in the XPS energy regime (more than several hundred eV) is that the scattering amplitude is strongly forward peaked. For this reason the qualitative interpretation of XPD spectra is relatively straightforward: maxima appear in the directions of the neighboring atoms. Another point to be kept in mind that Ni is a stronger scatterer than O because of its higher atomic number (cf. Refs. 10 and 11). Figure 10 shows the calculated intensities for scattering on a single atom for the two most important directions in the (001) plane: [001] and [101]. Besides maxima pointing into the direction of the scattering atom (zeroth order diffraction) we find modulations due to higher-order interference between outgoing and scattered waves.

Looking at the (010) XPD spectra in Figs. 3 and 4 the intensity maxima can be attributed to the four nearest-neighbor directions indicated in Fig. 4. These directions are [001], [103], [102], and [101] (0°, 18°, 27°, and 45°). In both, O $1s$ and Ni $2p$, there is a strong maximum in normal emission ([001]), where the atoms are most densely packed. The next-nearest neighbor is found under 45°/[101], where we observe a clear, sharp maximum for O $1s$ and a broad one for Ni $2p$.

The third maximum between 20° and 30° shifts from a

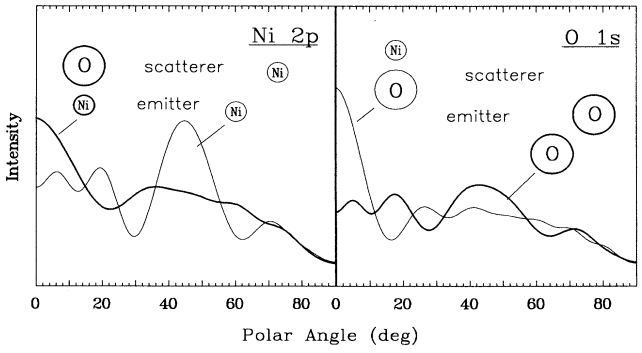

FIG. 10. Calculated intensities for scattering on one atom (the emitting atom is in the bottom). These pairs correspond to the closest neighbors in NiO.

higher angle in the O 1*s* spectrum to a lower one for Ni 2*p*. Figure 4 shows two directions to not so close neighbors within this range: [102] and [103]. Taking into account the different scattering strength of O and Ni we would expect a stronger contribution from the neighboring Ni atom, that means [102] for O 1*s* and [103] for Ni 2*p*. This is just what we observe experimentally, as can be seen in Fig. 4.

Additionally we have contributions from first-order diffraction ([001] and [101]) to these directions (see Fig. 10). In both cases we get additional intensity at about 20°, which is just the direction of the experimental maximum for Ni 2*p*. For O 1*s* we observe a broader maximum than for Ni 2*p* which could be due to this additional intensity.

A similar description can be given for the $1\bar{1}0$ spectra in Figs. 3 and 5. The nearest-neighbors' directions in this azimuth are [001], $[1\bar{1}3]$, $[1\bar{1}2]$, and $[1\bar{1}1]$. Again, there is a strong maximum in normal emission. For O 1*s* there is a maximum at around 30° which is inclined to the $[1\bar{1}3]$ Ni atom, and a weak maximum at around 40° pointing to the $[1\bar{2}3]$ atom (the top right Ni atom). But there is only a weak structure at 50°/$[1\bar{1}1]$. For Ni 2*p* there is, apart from the normal emission, a broad feature around 30°, whose maximum points to the $[1\bar{1}2]$ Ni atom. The $[1\bar{1}1]$ O atom also gives a clear contribution to a shallow but clearly visible maximum at around 50°.

To summarize: the main parts in the spectra are formed due to zeroth order scattering (forward focusing) on the neighbors of the emitting atoms. Additionally we observe contributions from first-order scattering near the strongest scattering directions. There are clear differences between the behavior of the O 1*s* and the Ni 2*p* emission. This is what we expect because the surrounding atoms are exchanged (each O is replaced by Ni and vice versa) and O and Ni differ strongly in their scattering strength.

C. Comparison with SSC calculations

However, we are left with a number of open questions concerning the relative intensities. For example, in the O 1*s* (010) spectrum the intensity at 45° is nearly as high (or higher if the photoionization cross section is taken into account) as the normal emission, but for Ni 2*p* this maximum is very shallow and much weaker than the normal emission. This is just opposite as what would be expected from the scattering strength of the atoms in these directions (O for O 1*s* and Ni for Ni 2*p*).

To get further insight into these problems we did SSC calculations as described above. Unfortunately the results of the calculations turned out to be not very encouraging in the beginning. As can be seen in the bottom of Fig. 11 simple SSC calculations do not very much resemble the measured data. At 45° they result in high intensity for Ni 2*p*, low for O 1*s*. In the calculation for O 1*s* this maximum is nearly invisible because of two neighboring maxima. Also the maximum in normal emission is much higher than the rest in both cases.

These problems are not a matter of cluster size. We increased the cluster size until we reached convergence, that means until there was no further change with size. So we had to look for other influences. As mentioned above, the two main shortcomings of basic SSC calculations are the neglection of spherical wave scattering and multiple scattering. To correct for spherical scattering it is common to simply reduce the scattering factors. We did this, but only for scattering by Ni. O is a weak scatterer with low atomic number Z, so these corrections do not have a big influence on the O scattering factor. The Ni scattering factor was diminished by a factor of 2.0. The result is shown in Fig. 11 and indicates a clear improvement.

The next step was to at least simulate multiple scattering as described above. These two corrections together

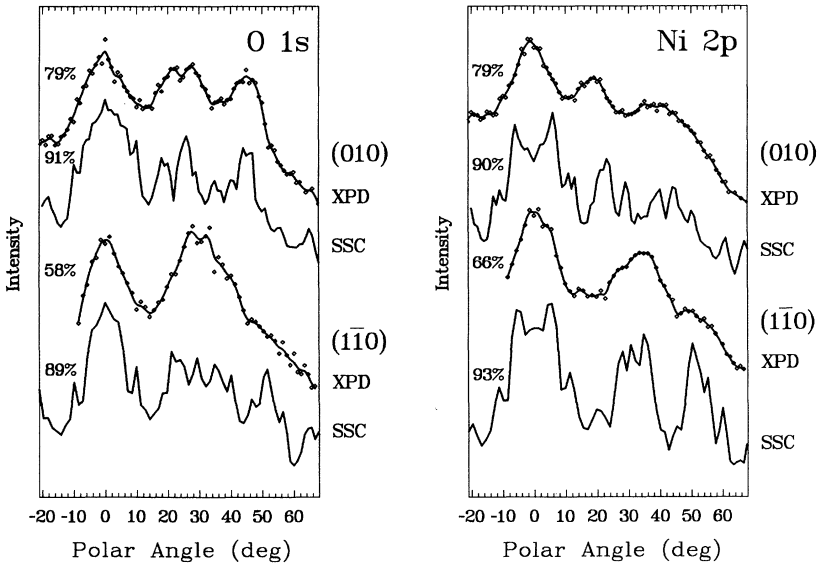

FIG. 11. Influence of a diminished Ni scattering factor (labeled Ni-Damping) and simulated multiple scattering (labeled MSC) on the calculated O 1*s* and Ni 2*p* (010) intensities.

give a much more convincing description of what is obtained experimentally. Figure 12 shows the final results together with the measurements.

The agreement is not perfect but the most important features are well described. Now there is much higher intensity at 45° for O 1*s*, and the opposite for Ni 2*p*. The calculation also accounts for the width of this maximum, giving a much broader maximum for Ni 2*p* than for O 1*s*. However, the maxima in the calculation for Ni 2*p* (010) seem to be shifted a bit.

Another discrepancy is that maxima at higher angles are not observed or strongly attenuated in the experiment. This is for angles above 60° in the (010) spectra and for angles above 45° in the $1\bar{1}0$ spectra. The reason for this is that the instrumental response is getting worse for glancing detection angles because the visible cross section of the sample surface gets smaller than the detected area of the analyzer.

D. Ion-bombarded NiO

The last point to discuss here is the effect of ion bombardment on the NiO surface. Photoelectron diffraction is closely connected to the ordering of the surface. If this ordering is reduced (e.g., by sputtering) we would expect that the diffraction features would be weakened as well. This is what we observe in Fig. 6. After the first sputter cycle the surface is disturbed slightly and the diffraction features only change little. After the second sputter cycle the two maxima around 20° and 45° are almost completely gone, at least in the Ni 2*p* spectrum.

However, the surface cannot be completely disordered because then there would be no maximum in normal emission. For a disorded (or a submonolayer) structure the intensity should only be influenced by the photoionization cross section and thus exhibit a broad maximum at an angle of 90° with respect to the incidence of light.

We do not observe this for the main peaks of O 1*s* and Ni 2*p* but for the O 1*s* satellite which indicates that the atoms from which the satellite electrons originate are situated on top of the NiO in a single layer or in disordered multiple layers without short-range order (otherwise they should exhibit diffraction effects). It is known from the results in Ref. 15 that this satellite feature in the sputtered O 1*s* XPS spectrum is due to OH that adsorbs on defects (in our case produced by ion bombardment). When using a nondifferentially pumped ion gun, as in our experiments, the surface gets contaminated from the residual gas.

The remaining modulation of the intensity of the main peaks, especially the maximum at 0°, indicates that the structure underneath this disturbed layer stays more or less intact, at least on a short-range scale. The layer on top attenuates emission from below. Inelastic attenuation is proportional to $\exp(-x/\lambda)$, where x is the traveled path and λ is the inelastic mean free path (see above). The traveled path is highest for high emission angles Θ ($\propto \cos\Theta^{-1}$). The consequence is that the off-normal maxima are reduced much stronger than the normal-emission maximum. This is what we observe in Fig. 6. The difference between the O 1*s* and the Ni 2*p* emission is probably due to the higher inelastic mean free path of the O 1*s* electrons (17.8 Å vs 13.1 Å).

VI. CONCLUSIONS

The qualitative explanation of the presented XPD spectra of NiO is rather straightforward. The main maxima can de deduced from the close-packed rows of atoms in the NiO structure. However, when it comes to a quantitative description, which means the interpretation of relative intensities of the XPD peaks, we run into difficulties. In studies of TiO_2 (Refs. 36 and 37) it was found

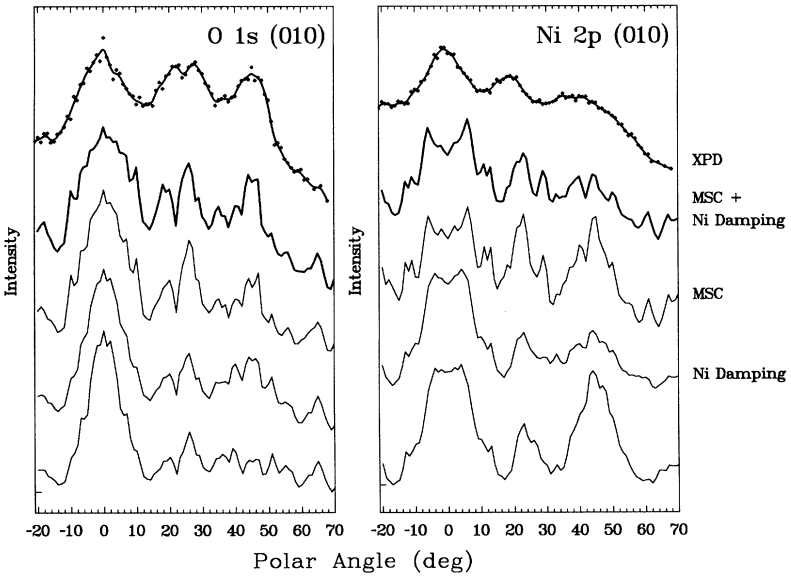

FIG. 12. Comparison of experimental XPD curves with SSC calculations including diminished Ni scattering factors and multiple scattering corrections.

that the scattering on O atoms only contributes little to the XPD spectrum, but we found that it has a very big influence as can be seen e.g. for the [101] emission in the O 1*s* XPD.

Simple single-scattering-cluster calculations do not give a reasonable explanation for the experimental observations. Additionally to diminishing the scattering factor for Ni we introduced an empirical correction to simulate multiple scattering. This results in a considerable improvement in the description of the experimental data. By our correction we avoided full-scale multiple-scattering calculations but nevertheless included this effect. Another advantage of our approach is that we did not completely sacrifice the simplicity of the SSC approach which is that the basic phenomena can be understood from looking at the crystal structure. From the results of the calculations we can judge that multiple scattering plays a very important role in understanding the diffraction features.

In spectra obtained from crystals bombarded with Ar ions off-normal maxima are weakened and vanish for higher doses of Ar ion bombardment. This effect is due to the adsorption of OH during the sputtering process on one hand and the destruction of the order of the top layer of the crystal. Both results in an attenuation of the emission from the deeper layer: the larger the off-normal angle the bigger is the influence. Because this layer is not well ordered it does not add a contribution to coherent scattering.

From the overall angular variation of the Ni 2*p* intensity we deduce a smaller asymmetry factor for the photoionization cross section than calculated for atomic emission. This is in good agreement with calculations presented in Ref. 33.

ACKNOWLEDGMENT

This work has been supported by the Deutsche Forschungsgemeinschaft through SFB 225.

[1] K. Siegbahn, U. Gelius, H. Siegbahn, and E. Olson, Phys. Lett. **32A**, 221 (1970).
[2] K. Siegbahn, U. Gelius, H. Siegbahn, and E. Olson, Phys. Scr. **1**, 272 (1970).
[3] C. S. Fadley, Prog. Surf. Sci. **16**, 275 (1984).
[4] C. S. Fadley, Phys. Scr. **T17**, 39 (1987).
[5] G. Grenet, Y. Jugnet, S. Holmberg, H. C. Poon, and T. M. Duc, Surf. Interf. Anal. **14**, 367 (1989).
[6] W. F. Egelhoff, Jr., CRC Crit. Rev. Solid State Mater. Sci. **16**, 213 (1990).
[7] S. A. Chambers, Adv. Phys. **40**, 357 (1991).
[8] S. A. Chambers, Surf. Sci. Rep. **16**, 261 (1992).
[9] W. F. Egelhoff, Jr., Phys. Rev. B **30**, 1052 (1984).
[10] M. Fink and J. Ingram, At. Data Nucl. Data Tables **4**, 129 (1972).
[11] D. Gregory and M. Fink, At. Data Nucl. Data Tables **14**, 39 (1974).
[12] H. C. Poon and S. Y. Tong, Phys. Rev. B **30**, 6211 (1984).
[13] C. Scharfschwerdt, J. Kutscher, F. Schneider, M. Neumann, and S. Tougaard, J. Electron Spectrosc. Relat. Phenom. **60**, 321 (1992).
[14] H. Kuhlenbeck, G. Odörfer, R. Jaeger, G. Illing, M. Menges, T. Mull, H.-J. Freund, M. Pöhlchen, V. Staemmler, S. Witzel, C. Scharfschwerdt, K. Wennemann, T. Liedtke, and M. Neumann, Phys. Rev. B **43**, 1969 (1991).
[15] S. Uhlenbrock, C. Scharfschwerdt, M. Neumann, G. Illing, and H.-J. Freund, J. Phys. Condens. Matter **4**, 7973 (1992).
[16] S. Tougaard, Surf. Sci. **216**, 343 (1989).
[17] M. A. Langell, Surf. Sci. **186**, 323 (1987).
[18] M. A. Langell, Nucl. Instrum. Methods **B28**, 502 (1987).
[19] S. Kono, S. M. Golberg, N. F. T. Hall, and C. S. Fadley, Phys. Rev. B **22**, 6085 (1980).
[20] M. Sagurton, E. L. Bullock, and C. S. Fadley, Surf. Sci. **182**, 287 (1987).
[21] J. Osterwalder, A. Stuck, D. J. Friedman, A. Kaduwela, C. S. Fadley, J. Mustre de Leon, and J. J. Rehr, Phys. Scr. **41**, 990 (1990).
[22] J. Cooper and R. N. Zare, J. Chem. Phys. **48**, 942 (1968).
[23] R. F. Reilman, A. Msezane, and S. T. Manson, J. Electron Spectrosc. Relat. Phenom. **8**, 389 (1976).
[24] I. M. Band, Y. I. Kharitonov, and M. B. Trzhaskovskaya, At. Data Nucl. Data Tables **23**, 443 (1979).
[25] J. J. Rehr, R. C. Albers, C. R. Natoli, and E. A. Stern, Phys. Rev. B **34**, 4350 (1986).
[26] J. Mustre de Leon, J. J. Natoli, C. R. Fadley, and J. Osterwalder, Phys. Rev. B **39**, 5632 (1989).
[27] K. G. Subhadra and D. B. Sirdeshmukh, Indian J. Pure & Appl. Phys. **16**, 693 (1978).
[28] S. Witzel, M. Neuber, M. Neumann, G. Timmer, and G. Borstel, BESSY Jahresbericht (Berlin), p. 197 (1989).
[29] S. Y. Tong, H. C. Poon, and D. R. Snider, Phys. Rev. B **32**, 2096 (1985).
[30] M.-L. Xu, J. J. Barton, and M. A. van Hove, Phys. Rev. B **39**, 8275 (1989).
[31] W. F. Egelhoff, Jr., Phys. Rev. Lett. **59**, 559 (1987).
[32] S. Tanuma, C. J. Powell, and D. R. Penn, Surf. Interf. Anal. **17**, 927 (1991).
[33] H. Ebel, M. F. Ebel, and A. Jablonski, J. Electron Spectrosc. Relat. Phenom. **35**, 155 (1985).
[34] A. Jablonski, Surf. Interf. Anal. **14**, 659 (1989).
[35] R. A. Armstrong and W. F. Egelhoff, Jr., Surf. Sci. **154**, 225 (1985).
[36] R. Heise, R. Courths, and S. Witzel, Solid State Commun. **84**, 567 (1992).
[37] B. Maschhoff, J.-M. Pan, and T. E. Madey, Surf. Sci. **259**, 190 (1991).